Quantification of Thermal Lensing Using an Artificial Eye

Erica L. Towle, Mike Rickman, Andrew K. Dunn, Ashley J. Welch, and Robert J. Thomas

***Abstract*—Recent experiments have concluded that it is possible to interrupt the vision of human subjects using infrared (IR) light through an effect known as thermal lensing. While these experiments successfully demonstrated the influence of thermal lensing on an Amsler grid target, little has been done to quantify the amount of visual disruption resulting from this phenomenon. Therefore, an artificial eye system was configured to better quantify the refractive power of the thermal lens generated within the human eye. The influence of 1319 nm energy with power levels from 220 to 630 mW and exposure durations between 0.25 and 1.00 s was evaluated based on changes induced within a visible probe beam (542 nm). Results showed up to a –2.0 D blur could be induced in human subjects using these energy levels. Results also established a relationship between the peak IR power and exposure durations used to determine the strength of the thermal lens.**

***Index Terms*—Cain cell, laser-tissue interaction, nonlinear optics, thermal blooming.**

I. Introduction

LAW enforcement and military personnel are constantly researching new ways to safely stop potential threats without the use of lethal force. Nonlethal weapons (e.g., tasers, spike strips, ocular interruption devices, etc.) serve a vital role in the success of a mission, and have been shown to minimize casualties and collateral damage in a variety of situations. The effect of thermal lensing in ocular media has been under investigation for the last few years as a potential new form of ocular interruption device [1]–[8]. While previous research has demonstrated the potential of such a device, additional experimental studies are needed before the full potential of using thermal lensing as a nonlethal weapon can be understood.

Recently, an investigation was conducted in which human subjects were exposed to an infrared (IR) laser (1319 nm) at various power levels (86.5–692.4 mWcm^{-2}) and exposure durations (0.25–1.00 s) [7]. This study concluded that it was possible to induce the significant blurring of human vision using the thermal lensing effect when sufficiently high power levels were used. Since the overall goal of the previous study was to grossly demonstrate that thermal lensing can safely and effectively alter human vision, very little was done to accurately quantify the amount of blur or shift in visual performance resulting from thermal lens [7]. Therefore, an experimental investigation using an artificial eye was conducted using IR laser parameters similar to the previous study to obtain a more accurate measurement of the thermal lensing effect under these

Manuscript received January 3, 2013; revised April 1, 2013; accepted April 22, 2013. Date of publication May 15, 2013; date of current version August 29, 2013.

E. L. Towle is with the Air Force Research Laboratory, Fort Sam Houston, TX 78234 USA and also with the Biomedical Engineering Department, University of Texas at Austin, Austin, TX 78712 USA (e-mail: eweber@utexas.edu).

M. Rickman is with the Department of Biomedical Sciences and Technologies, TASC, Inc., San Antonio, TX 76010 USA (e-mail: john.m.rickman.ctr@mail.mil).

A. K. Dunn and A. J. Welch are with the Department of Biomedical Engineering, University of Texas at Austin, Austin, TX 78712 USA (e-mail: adunn@mail.utexas.edu; welch@mail.utexas.edu).

R. J. Thomas is with the Air Force Research Laboratory, Fort Sam Houston, TX 78234 USA (e-mail: robert.j.thomas251.civ@mail.mil).

Color versions of one or more of the figures in this paper are available online at http://ieeexplore.ieee.org.

Digital Object Identifier 10.1109/JSTQE.2013.2260728

II. Background

In general, the principle of thermal lensing refers to the heating of a transparent material (e.g. water, air, fused silica, ethanol, etc.) such that a change in the index of refraction is induced

$$n\left(r,z,t\right)=n0\left(r,z,t\right)+\frac{\partial n}{\partial T}+f\left(T\left(r,z,t\right)\right) \qquad (1)$$

where $n\left(r,z,t\right)$ is the spatial and temporal index of refraction under a thermal lens, n_0 is the baseline index of refraction, dn/dT is the thermooptic coefficient of the material, and $T\left(r,z,t\right)$ is the space and time varying change in temperature induced within the material. This change in temperature is highly dependent on wavelength, space, and time. The laser wavelength will determine the amount of energy absorbed in the material, the spatial beam profile of a laser (Gaussian, top hat, etc.) will impact the way energy is spatially deposited within the media and the exposure duration will control the total energy (heat) delivered to the media.

The thermal lensing phenomenon is commonly known to occur in high powered lasers, where the heat generated within the gain media (e.g., crystal) causes a change in the media's index of refraction and results in a poor quality laser. These changes can manifest in many ways depending on the thermooptic coefficient of the material. In the human eye, the thermooptic coefficient is approximately equal to $-7.82\times10^{-5}\mathrm{K}^{-1}$; therefore, a thermal lens generated in the eye results in the formation of a negative focal length-like lens which elongates the natural focus of the eye. This implies light entering the eye then focuses slightly behind the retina. Since light is no longer sharply focused on the retinal plane, a distortion from normal vision is observed.

In order to achieve thermal lensing in the human eye, a source must be chosen with the proper wavelength, so the energy is absorbed gradually within the media to avoid damage. Previous research has shown that in the near infrared range, between 1150 and 1400 nm, the absorption coefficient of the eye is sufficiently low to allow energy to propagate through the eye,

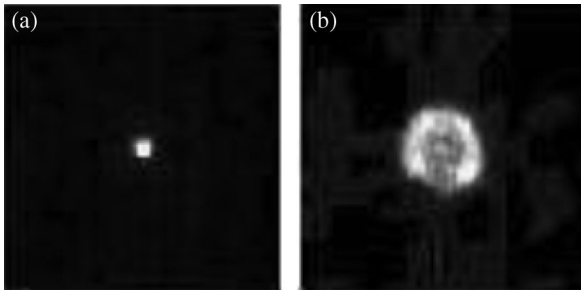

Fig. 1. Visible focal region spot of HeNe laser co-aligned with a 150 mW 1318 nm laser at (a) initial state ($t = 0$ s) and (b) the end of the IR-laser exposure ($t = 1.0$ s). Measurements were made in an artificial eye [2].

yet high enough that less than 15% of the energy within this range will reach the retina [9]. This energy is gradually absorbed throughout the eye creating a gradient of temperature change with energy levels which are well below the damage threshold [7], [10].

Previously, an artificial eye model, known as the Cain Cell, was used to measure the influence of thermal lensing induced by several different IR wavelength lasers between 1150 and 1318 nm [2]. Changes in a visible probe beam size at various axial locations within the artificial eye were monitored under the different thermal lensing conditions. These studies demonstrated a distinct blooming of the visible beam within the media, see Fig. 1, and a focal shift which was used to measure the strength of the thermal lens in dipoters (D).

While the experiment by Vincelette *et al*. was able to determine relationships between IR wavelength and energy levels with the refractive power of the thermal lens, this study was limited as it indirectly measured the changes within the artificial eye and only considered exposure durations of 1 s [2]. The indirect method of imaging the visible probe beam led to a low-resolution image which may mask some of the subtle effects of the thermal lens on the beam profile. Since the experiment also only considered 1 s exposure durations, it would be difficult to make a direct comparison to the various exposure durations and power levels used in the human effects study. Therefore, this paper describes a more detailed artificial eye study conducted so that the thermal lensing effects induced in human subjects can be more comprehensively compared.

III. Methods

A. Artificial Eye: Modified Cain Cell

To overcome some of the limitations of the artificial eye used in previous experiments, a fiber-based system was developed to facilitate direct measurements of changes in a visible beam within the artificial eye [8]. With the endoscopic system, changes in beam shape and/or intensity can be measured directly at any 3-D spatial point within the cell. To ensure the adequate alignment of the fiber bundle to the center of the artificial eye and allow for precise movements of the fiber bundle along the axial length of the cell, the fiber was mounted to an automated translation stage (via a custom designed adapter). For these experiments, the artificial eye was filled with distilled water. Since

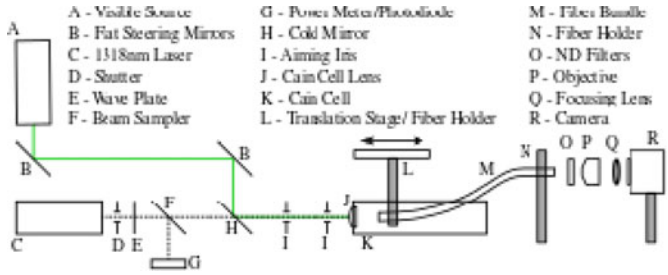

Fig. 2. Artificial eye experimental setup.

the optical properties of vitreous and water are roughly the same, this should not impact the accuracy of the model [11].

B. Experimental Setup

The experimental setup, shown in Fig. 2, used a cold mirror (H) to coalign the visible (A, 5.1 mm diam., 542 nm) and IR (C, 4.5 mm diam., 1319 nm, C) laser beams and center them on the artificial eye lens (J). Prior to placing the artificial eye in the system, the $1/e^2$ beam diameter was measured using Spiricon LBA 300-PC beam profiling software (Spiricon, Inc., Logan, UT, USA) connected to either a CoHu 4800 (Cohu Inc, Poway, CA, USA) for the visible laser or sensors SU320M (Sensors Unlimited, Inc., Princeton, NJ, USA) for the IR laser. Two separate cameras were required to obtain a clear image of both beam profiles; however, small traces of visible light could be detected on the SU320M camera, so it was also used to confirm coalignment of the lasers positions. During these measurements, the lasers were also left on for long periods of time (>60 s) to observe any changes in the beam shape resulting from a thermal lens generated from heating the optical mirrors. These measurements showed no significant changes in either beam profile, and, therefore, any result of thermal lensing generated from the experiment must come from a thermal gradient within the artificial eye.

The fiber bundle (M) was positioned within the cell (K) and mounted on translation stages (L) so that the position within the cell could be accurately adjusted to the focal plane. The back end of the fiber was focused to an 8-bit monochromatic camera-link camera (R, MV-D1024–160-CL-8, Photon Focus AG, Lachen Switzerland, 100 Hz) using a 10× infinity-corrected objective (P, M Plan Apo 10, Mitutoyo, Aurora IL, USA) combined with a 200 mm plano-convex lens (O, LA708, Thorlabs, Newton, NJ, USA). The secondary lens was manually offset from the focus of the objective to yield a resulting image of approximately 2 mm^2 with individual pixel resolution of 0.0012 mm per pixel. Neutral density filters (O) were placed in front of the camera to reduce the saturation of the image.

Prior to any data collection, the visible beam was first turned on and propagated through the cell for a minimum of 5 min to allow the beam to stabilize. Following that, a 1 s time delay from the start of data acquisition was applied so that a baseline of the visible beam diameter could be obtained for each power level used. The exposure duration of the IR beam was controlled using an electronic shutter (D, Uniblitz, Rochester, NY, USA), and the irradiance of the IR beam was controlled using a

half-wave plate (E) and polarizing beam splitter cube (F). One output of the beam splitter cube was used for a continuous monitor of IR power (G) while the other path was used for the experiment. The IR power levels of 220, 350, and 630 mW and exposure durations of 0.50, 0.75, and 1.00 s were chosen to maintain consistency with previous human experiments [7]. The power of the visible beam was set so that the focused beam maximized the full dynamic range of the camera (approx. 1 μW).

C. Image Processing

Image sequences were collected using Streampix 5 software (Norpix, Inc., Montreal, QC, Canada). In order to properly synchronize the acquisition of each frame with the IR laser exposure, an NI USB-6201 data acquisition (DAQ) board (National Instruments, Austin, TX,) was used to trigger each frame of the camera, start and stop image recordings in the software, and control the pulse duration of the Uniblitz shutter. A simple LabView (National Instruments, Austin, TX, USA) program was developed to coordinate and record all of the signals on the DAQ board.

For each image collected, the strength of the thermal lens was assessed by measuring the change in the visible beam diameter as a function of time. During the effect, the intensity of the images decreased such that the beam became difficult to analytically distinguish from the image background. To improve the signal-to-noise (SNR) ratio, the photon focus camera was set to LinLog mode with skimming. The advantage of the LinLog mode was that as the intensity reached the upper boundary of the sensor, the camera switched to a logarithmic compression, decreasing the likelihood of saturating the camera at higher intensities. Skimming, another property of the camera, enhanced the dark areas of an image by adjusting the in-pixel gain for low signal levels. The combination of skimming with the LinLog capability allowed the camera to capture a much higher dynamic range without needing to alter the camera's exposure time which would limit the maximum frame rate. These changes greatly improved the appearance of the visible beam as it focused and bloomed within each frame. However, further improvements to the SNR were still needed to adequately measure the dynamics of the thermal lens. Therefore, datasets were also collected in pairs with slight adjustments of the lateral fiber position with each trial, which was accomplished using a manual translation stage. These images were then averaged together in order to minimize scattering and pixelization from the fiber bundle itself. Finally, the baseline noise of the camera was measured and averaged across ten frames. This noise was subtracted from each collected image to further improve the resulting analysis.

As the visible beam changed with the generated thermal lens, it deformed and became very non-Gaussian, see Fig. 3. This change in beam shape made it difficult to measure the diameter of the visible beam as a function of time. Several different beam measurement methods (Gaussian Fit, D4σ, etc.) were tried; however, the most reliable solution was to measure the $1/e^2$ diameter of the beam by assessing the points of the beam profile, where the intensity of the beam was greater than $I_{\max}/e^2$. This method gave reasonable estimations of the beam size as a function of space and time when compared to visual inspection of the images, and was robust enough to overcome any remaining noise which might be present within the images during the effect.

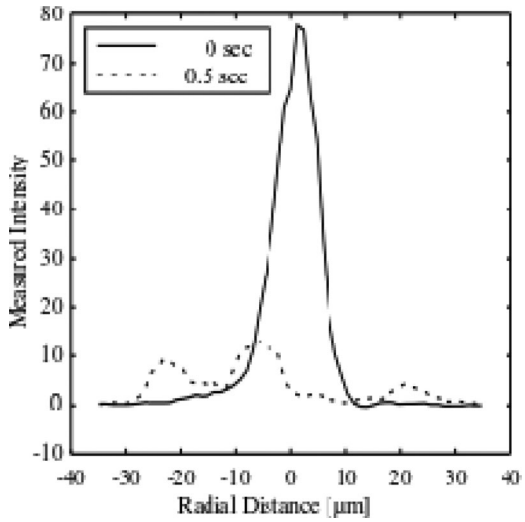

Fig. 3. Example nonuniform visible beam profile at the focal plane resulting from thermal lensing after the IR light (630 mW) was turned on for 0.5 s.

D. Calculating the Power of the Thermal Lens

To calculate the power of the thermal lens generated with each IR laser exposure, the focal length of the new system (artificialy eye + thermal lens) was first determined by extracting the angle of focus θ, according to the following equation:

$$\theta = \tan \frac{w(z_1) - w(z_2)}{z_1 - z_2} \tag{2}$$

where $w(z)$ was the beam waist at axial position z. This calculation of the angle was then used to approximate the focal length of the system, $f_{\rm sys}$, based on the original diameter of the visible beam, D

$$f_{\rm sys} = D/\theta. \tag{3}$$

Based on computational work conducted in conjunction with these experiments, a dominate thermal lensing effect produced in the eye occurs approximately 0.2 mm behind the front surface of the cornea. Using a thin lens approximation in conjunction with the total focal length of the system, the approximate power of the thermal lens could be calculated as

$$\frac{1}{f_{\rm sys}} = \frac{1}{f_{\rm lens}} + \frac{1}{f_{\rm tl}} - \frac{d}{f_{\rm lens} f_{\rm tl}} \tag{4}$$

where $f_{\rm lens}$ denotes the original focal length of the artificial eye, $f_{\rm tl}$ denotes the focal length of the thermal lens, and d represents the distance between the two lenses.

IV. Results

A. Quantification of "Blooming" at the Artificial Retinal Plane

Fig. 4 shows a sequence of images of the focused spot within the artificial eye during one pulse of the IR light (220–630 mW,

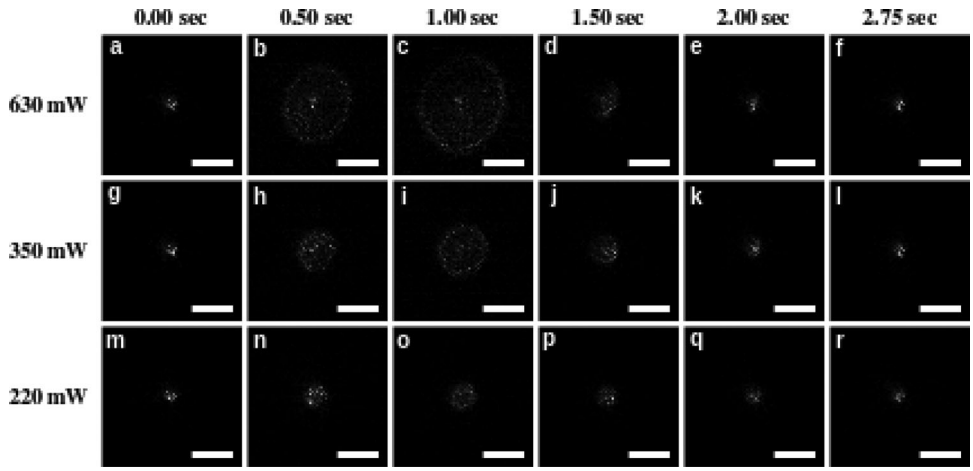

Fig. 4. Images collected at the focal plane of the artificial eye shown at various points during the induced thermal lens. IR power was varied from 220 to 630 mW. The IR light was turned on at $t = 0.0$ s and closed 1.0 s later. Scale bars indicate 50 μm.

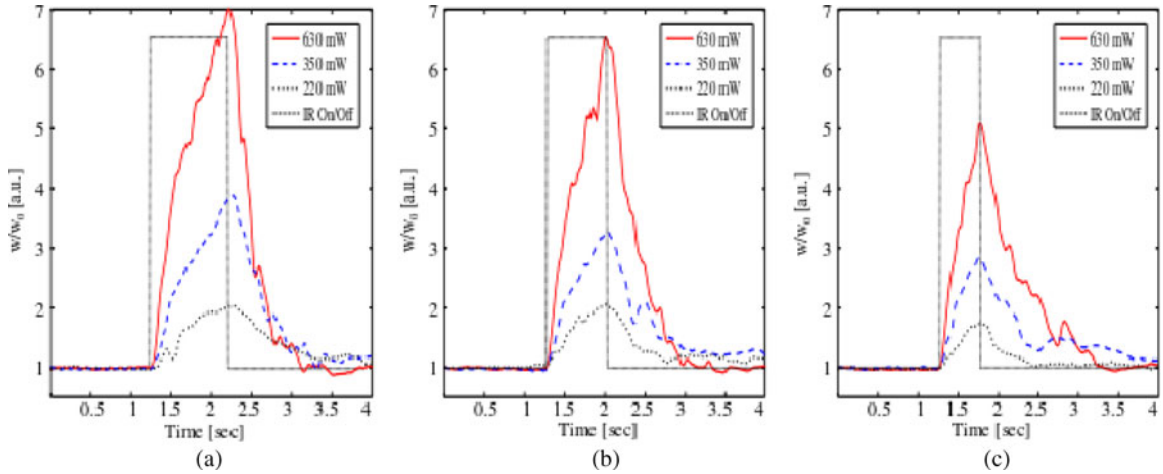

Fig. 5. Temporal changes in the normalized focused beam diameter (w/w0) as a function of infrared power (220–630 mW) with different IR exposure levels (0.50– 1.0 s).

1.0 s exposure). From these images, it was clear that as the thermal lens formed within the media, the focused spot size of the visible beam expanded and the intensity of the beam within each pixel decreased; however, the average power across the frame remained constant. After the laser was ON for 1.0 s, the irradiance of the focused spot at the highest IR power level [630 mW, Fig. 4(a–e)] had become so diffused over the lateral area that it became difficult to distinguish from noise of the camera if the color map of the image was not dynamically scaled. For the lower IR power levels, the visible beam distinctly bloomed [see Fig. 4(i) and (o)]; however, the overall magnitude of the blooming decreased with the input IR power level. Once the IR laser was shuttered off ($t = 1.00$ s), the artificial eye began to cool and the visible spot returned to its natural state ($t = 2.75$ s).

To better understand the dynamics of the thermal lens, the beam diameter of the focused visible laser was measured for each power level and exposure duration; see Fig. 5. The first noticeable effect was the strong relationship between the power in the system and the effective bloom of the focused beam; with the most blooming (approximately 7×) at the highest energy level (630 mW, 1.00 s). As the exposure duration was decreased, the blooming of the beam also decreased suggesting that there was a relationship between the irradiance of the IR beam as opposed to the exposure duration alone. The relationship between irradiance and exposure duration was further analyzed in Fig. 6(a), where the maximum blooming (change in beam diameter) was plotted for each of the various power levels and exposure duration.

For each set of exposure durations, an exponential curve fit best described the changes. These fits are described as

$$w_{\text{norm}} = \begin{cases} 1.15e^{0.0024p} \text{ for } t_{\text{exp}} = 0.50\ s \\ 1.24e^{0.0026p} \text{ for } t_{\text{exp}} = 0.75\ s \\ 1.38e^{0.0026p} \text{ for } t_{\text{exp}} = 1.00\ s \end{cases} \quad (5)$$

where p was the measured power (in mW) and t_{exp} was the exposure duration. From (5), it was clear that there was very little change in the slope of the exponential; however, the amplitude does shift slightly. This implies that the rate of the increase in

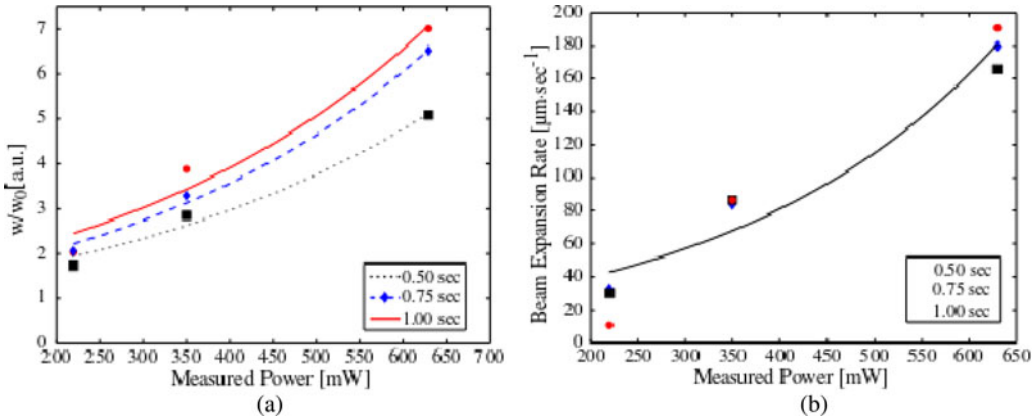

Fig. 6. (a) The maximum calculated change in beam diameter as a function of power and exposure duration with exponential fits and (b) the calculated change in beam diameter over time as a function on input power and exposure duration with average exponential fit.

TABLE I
RELAXATION TIME OF THE THERMAL LENS MEASURED AS THE AMOUNT OF TIME TAKEN FOR THE MAXIMUM BLOOMED VISIBLE BEAM AT THE RETINAL PLANE ($z = 0$) TO RETURN TO ITS INITIAL BEAM DIAMETER

		Power		
		220 mW	350 mW	630 mW
Exposure Duration	0.50 sec	1.01sec	1.72 sec	1.26 sec
	0.75 sec	1.01 sec	1.06 sec	1.01 sec
	1.00 sec	1.01 sec	1.01 sec	1.01 sec

beam diameter was more strongly influenced by the power of the IR beam rather than the exposure duration. This result was expected as the maximum achieved blooming would increase with duration of the exposure until the system reached steady state; however, the rate of the blooming will depend on the rate in which heat was deposited within the artificial eye (IR power).

Fig. 5 also demonstrates that the blooming of the visible beam began very quickly after the IR light was introduced to the system. On average, the amount of time for the beam diameter to bloom one standard deviation above the average baseline was 0.0178 ± 0.0097 s, implying that the artificial eye was very sensitive to even the smallest temperature change. Surprisingly, the power level did not influence the time to bloom for each case; however, this measurement was limited to the frame rate of the camera (100 Hz or 0.01 s). The rate of blooming was calculated under the various conditions, and as expected, the rate of increase in beam diameter was also very similar between exposure durations as shown in Fig. 6(b).

Once the IR light was turned OFF, the relaxation time was dependent on the thermal properties of the material as well as the volume heated. Table I depicts the relaxation time measured for each IR energy level.

The relaxation time of the thermal lens (as measured by the time taken for the bloomed beam diameter to return within 1 μm of the baseline), was the same for most of the experimental trials. On average the time taken for a visible beam to return to its initial beam diameter was 1.18 ± 0.1 s. Since the relaxation times were so similar despite larger beam diameters generated with higher energy cases, this suggested that the relaxation rate of each condition was very different. In other words, cases where the beam was largest would have a faster relaxation rate than beams which did not expand as greatly because the spatial distribution of the cooling was different.

B. Quantification of the Induced Focal Shift

In order to quantify the focal shift induced as a result of the thermal lens, measurements of the blooming visible beam were also taken at five axial positions within the artificial eye: -0.2, -0.1, 0, 0.1, and 0.4 mm, where negative values corresponded to movements closer to the lens and $z = 0$ related to the focal point of the artificial eye. For each position, data was again collected at the various power levels (220, 350, and 630 mW) for three different exposure durations (0.50, 0.75 and 1.00 sec).

Fig. 7 shows the captured images at each z-axis position after the IR laser had been left on for 1.00 s. From the images it was clear that as the IR light was added to the system, the focus of the visible beam shifted away from the artificial eye lens (deeper into the eye). As the power of the IR laser also increased, the magnitude of the shift in the focal point also seemed to increase. Similarly, to the retinal plane ($z = 0$) image analysis, the temporal change in beam diameter as a function of power was calculated for each axial position. These dynamics are shown in Fig. 8 for the 1.00 s exposure duration.

The temporal profiles at each axial location gave a very clear depiction of the shift in the focal point which occurred as the media was heated. For axial positions closer to the artificial eye lens [see Fig. 7(a) and (b)], the visible beam diameter increased as a function of the IR laser power. Since these positions in front of the focal plane only expand, it was inferred that the thermal lens generated was (1) always negative and (2) influences light in front of the retinal plane. In contrast, axial positions behind the retina showed the visible beam coming to a smaller spot (focusing). From the graph, it was clear that higher IR powers led to an initial focus of the visible beam; however, as the thermal lens power increased the focus of the visible beam continued to shift, and the visible beam blooming was again observed. The lowest power level (220 mW), however, decreased and remained a more focused beam. This further demonstrated that as the power and exposure duration were varied, the strength of the thermal lens was also changed.

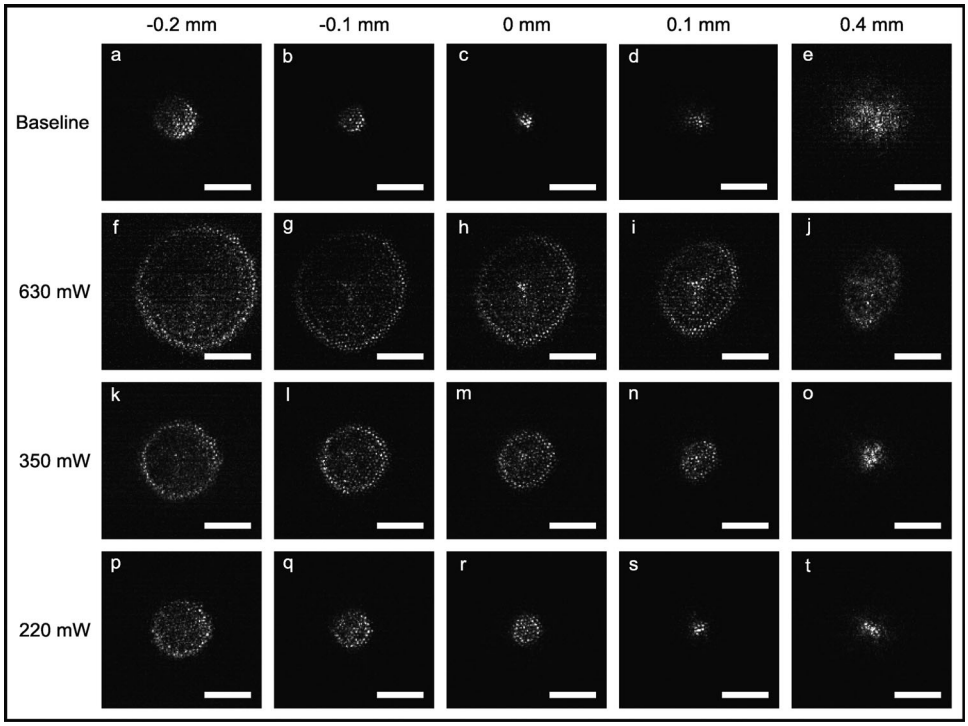

Fig. 7. Images taken at each z-axis position after the IR laser has been left on for 1.00 s for power levels of 220, 350 and 630 mW. Scale bars indicate 50 μm.

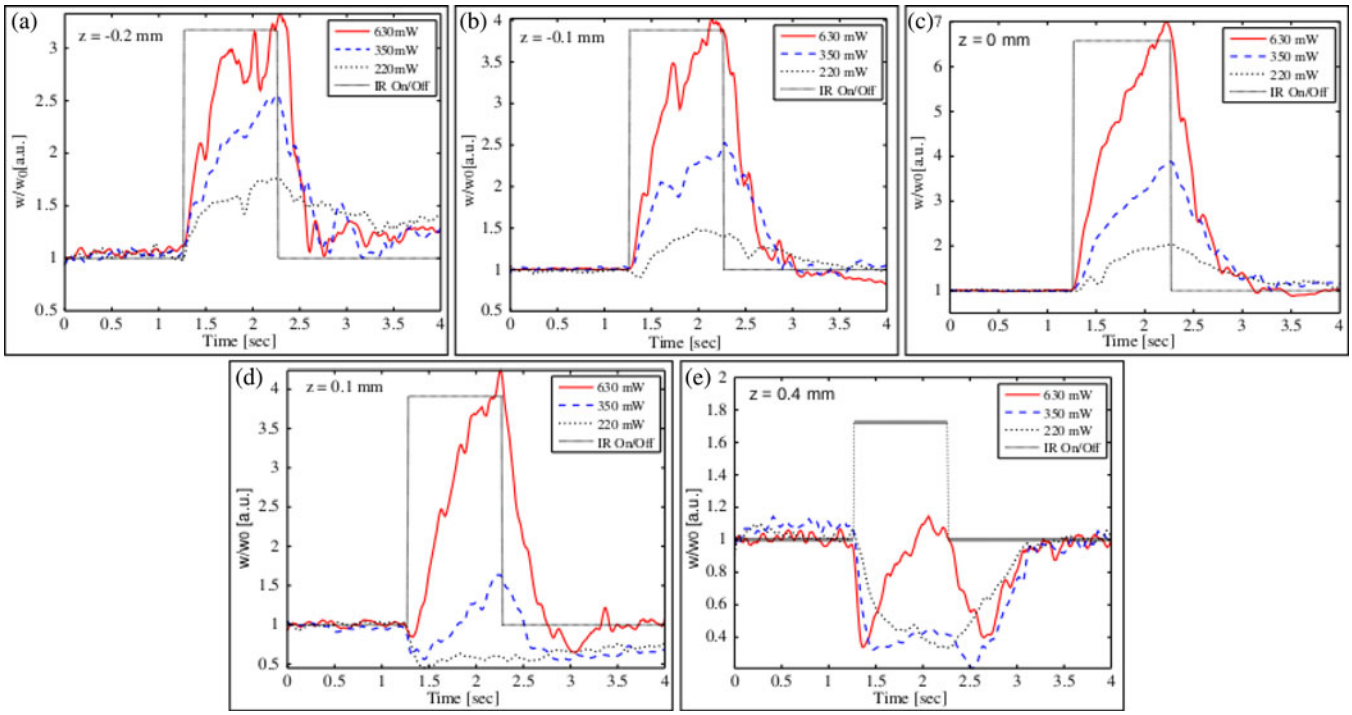

Fig. 8. Temporal changes in normalized beam diameter (w/w0) as a function of infrared power (220–630 mW) at different axial positions for an IR exposure duration of 1.00 s.

The maximum change in the beam as a function of axial (z) position was also analyzed; see Fig. 9(a). For the lowest power (220 mW) the maximum amplitude of the bloom did not appear to vary with exposure duration; however, at higher irradiance levels the exposure duration did begin to influence the diameter of the beam.

Finally, for each power and exposure duration condition, the power of the thermal lens was calculated; see Fig. 9(b). For

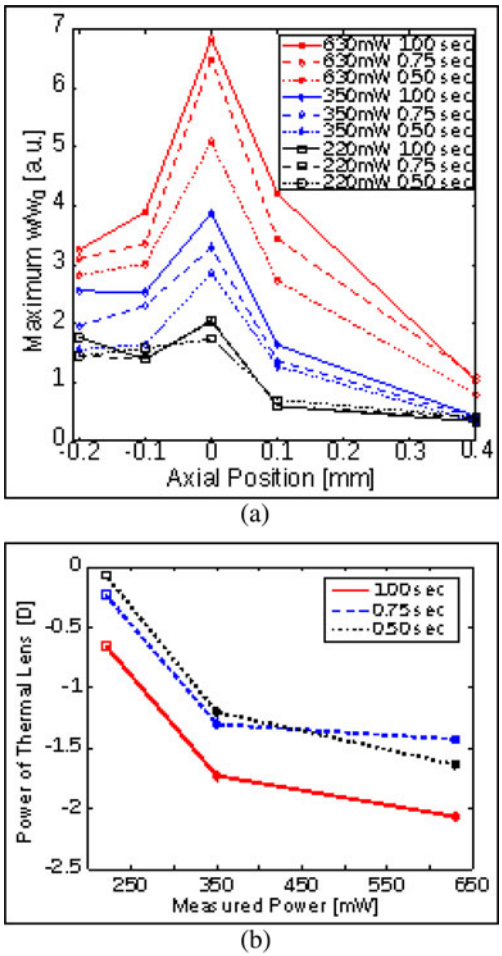

Fig. 9. (a) The maximum change of the visible profile as a function of axial position for all power levels and durations and (b) the calculated power of the thermal lens as a function of IR power and exposure duration.

the different exposure conditions used in this study, the overall power of the thermal lens was found to vary between −0.07 and −2.07 diopters (D). This power of thermal lens related to an elongating of the focus of the eye between 0.02 and 0.69 mm. As expected, the calculated power of the lens as related to IR power followed a similar positive relationship (increase IR power, increase absolute power of the thermal lens).

The 0.75 s duration conditions had a similar effect to the 0.50 s conditions despite the increase in energy of the beam. On first glance, this appeared as an inaccuracy of the data; however, upon further review the nonlinearity of the system was easily explained. During the higher powered long-exposure conditions the beam focus shifted through each axial position; see Fig. 8(d) and (e). In other words, the visible beam diameter at axial points beyond the focus initially shrunk down to a small spot, but as the strength of the thermal lens continued to increase, the beam diameter began to bloom again (in some cases beyond its original size). This increased beam diameter caused an artificial increase in the focusing angle, θ, which led to a decrease in the calculated power of the thermal lens. A similar effect was observed for the 1.00 s conditions; however, the resulting beam was always larger than the initial beam diameter, so the shift in focal length was consistently underpredicted.

V. Discussion

These experiments successfully measured the theoretical power of a thermal lens which was induced during human subject trials. Similar to the human experiments, the effect of the thermal lens on a visible beam was highly dependent on both power and exposure duration of the IR laser. The rate of expansion of a visible beam was closely related to the power level, while the maximum expansion was influenced by the duration of the exposure. As predicted from previous experiments, the rate of blooming was related to the change in temperature which increased proportionately to the total power delivered to the system. The average on-set time (time taken for the beam to bloom greater than one standard deviation above the baseline beam diameter) was measured to be 0.0178 ± 0.0097 s. While the temporal resolution of the camera was not fast enough to accurately resolve the onset time between the different power levels, the on-set time was still shown to be much faster than the accommodation time of the eye (300 ms) [12]. This would suggest that any effects that the IR laser has on vision would occur before the eye was able to accommodate for the change, and, therefore, accommodation would not be able to overcome the induced blur.

These experiments were also able to measure relaxation time of the thermal lensing effect (1.18 ± 0.15 s). The averaged measured relaxation time was shorter than previous reports of thermal lens decay in the cornea of 2.3 ± 0.1 s [13]. The artificial eye used in this experiment was a much larger open system compared to the natural eye. Therefore, it was much easier for the heat generated in the artificial eye to dissipate through the top of the container or via convective currents generated within the water of the cell. In addition, the lens of the artificial eye is a glass (SF-11) custom lens which will absorb significantly less energy than a traditional human eye. In contrast, the extracted cornea layer used in the study by Venkathesh *et al*. [13] retained its natural absorption and diffusion properties which allowed for heat generated within the layers to dissipate naturally. Therefore, while a relaxation time was measured in the artificial eye, it is concluded that the physical properties of the glass lens used in the artificial eye made this relaxation measurement less accurate. To overcome this limitation, future artificial eyes will incorporate more realistic materials (acrylic, PDMS, Peg, etc.) which will respond to temperature changes more closely to the human eye.

Axial measurements of the effect demonstrated a transient negative lens which is generated within the eye. In other words if more energy was added, the total observed blooming at the original focal plane will continue until a thermal equilibrium is reached. This implies that there is a maximum level of induced distortion possible for each power level, and there would be no benefit to continue to irradiate the tissue past this point as the influence on visual function would not increase but the risk of damaging the tissue would increase. For exposure durations and power levels used in this experiment; however, a thermal

equilibrium was not achieved so this was not a problem during the previous human-use trials.

Results of the experiment also showed that a refractive error between −0.07 and −2.07 diopters (D) was induced via the thermal lensing effect. The United States Air Force limits the uncorrected visual acuity of their pilots to no greater than −1.50 D in either eye. This suggests that if a pilot were to experience the effects of thermal lensing induced with a power level between 350 and 630 mW and an exposure duration longer than 0.75 s that individual would not maintain accurate visual acuity to meet the safety standards required to effectively pilot the aircraft. This correlates well with the visual disruption observed during the human use trials. Therefore, it can be concluded the strength of the thermal lens is fully capable of significantly altering visual performance without damaging the eye.

In the natural world, the axial length of the human eye has been known to vary as much as 11.7 mm (19.47 – 31.17 mm) [14] depending on a range of factors including subject ethnicity and age. For corrected vision, the perception of the thermal lens would be roughly the same across all subjects as the focus of light entering the eye would fall in relatively the same position. For the uncorrected eye, however, small changes in focal length induced by the thermal lens (between 0.02 and 0.69 mm) could potentially improve the focusing to a myope (near-sighted individual, light focuses in front of the retina) or increase the blur of an image to a hyperope (far-sighted, light focuses behind the retina). This distinction is important as the influence of a thermal lens would change depending on the target's ethnic background, age, and level of optical correction (glasses etc). In some cases, a device using this technology could increase the level of potential risk from a coaligned visible source if a lower powered thermal lens was induced which completely corrected for vision impairments.

VI. Conclusion

Experiments using a modified artificial eye have successfully measured the rate of visible beam expansion and decay resulting from thermal lensing, and determined the effective focal shift of a visible beam as a result of induced thermal lensing. By introducing a fiber bundle to the artificial eye, it was possible to obtain direct images of the changes in a coaligned visible beam which were then used to correlate the total IR energy needed to the strength of the induced thermal lens. As a result of this research, it can be concluded that it is possible up to a −2.0 D blur was induced in human subjects during the previous experiment. Results of these experiments also established a general relationship between the peak IR power and exposure durations used to the strength of the thermal lens.

Acknowledgment

The authors would like to thank Dr. R. Vincelette, Dr. T. Milner, and Dr. G. Rylander for their assistance and guidance in preparing for this project.

References

[1] R. L. Vincelette, B. A. Rockwell, J. W. Oliver, S. S. Kumra, R. J. Thomas, K. J. Schuster, G. D. Noojin, A. D. Shingledecker, D. J. Stolarski, and A. J. Welch, "Trends in retinal damage thresholds from 100 millisecond near-infrared radiation: A study at 1100, 1130, 1150 and 1319 nm," *Lasers Surg. Med.*, vol. 41, no. 5, p. 352, 2009.

[2] R. L. Vincelette, J. W. Oliver, B. A. Rockwell, R. J. Thomas, and A. J. Welch, "Confocal imaging of thermal lensing induced by near-infrared radiation in an artificial eye," *IEEE J Selected Topics Quantum Electron.*, vol. 16, no. 4, pp. 740–747, Jul./ Aug. 2010.

[3] R. L. Vincelette, J. W. Oliver, B. A. Rockwell, R. J. Thomas, and A. J. Welch, "Thermal lensing from near-infrared laser radiation in an artificial eye," *Proc. SPIE*, vol. 7175, p. 9, 2009.

[4] R. L. Vincelette, B. A. Rockwell, A. J. Welch, and D. J. Lund, "Thermal lensing in ocular media exposed to continuous-wave near infrared radiation: 1150–1350 nm region," *J. Biomed. Optics*, vol. 13, p. 054005, 2008.

[5] R. L. Vincelette, J. W. Oliver, G. D. Noojin, K. J. Schuster, A. D. Shingledecker, and A. J. Welch, "Method for measuring ocular aberrations induced by thermal lensing in vivo," *Proc. SPIE*, vol. 7562, 2010.

[6] R. L. Vincelette, R. J. Thomas, B. A. Rockwell, C. D. Clark, and A. J. Welch, "First-order model of thermal lensing in a virtual eye," *J. Opt. Soc. Amer. A*, vol. 26, no. 3, pp. 548–558, 2009.

[7] E. L. Towle, P. V. Garcia, P. A. Smith, R. J. Thomas, A. K. Dunn, A. J. Welch, and B. K. Foutch, "Visual disruption using the thermal lensing effect in the human eye: A pilot study," *J. Biomed. Opt.*, vol. 17, no. 10, 2012.

[8] E. L. Weber, M. Rickman, A. K. Dunn, A. J. Welch, and R. J. Thomas, "Direct assessment of thermal lensing in ocular media using an artificial eye," *Proc. SPIE*, vol. 8221, 2012.

[9] E. F. Maher. Transmission and absorption coefficients for the ocular media of the rhesus monkey. USAF School of Aerospace Medicine, TX, USA, Technical Rep., SAM-TR-78-32, 1978.

[10] J. A. Zuclich, D. J. Lund, and B. E. Stuck, "Wavelength dependence of ocular damage thresholds in the near-ir to far-ir transition region: Proposed revisions to mpes," *Health Phys.*, vol. 92, no. 1, pp. 15–23, 2007.

[11] R. L. Vincelette, "Thermal lensing in ocular media," Ph.D. dissertation, Univ. Texas at Austin, Austin, TX, USA, 2009.

[12] W. N Charman, "The eye in focus: Accommodation and presbyopia," *Clin. Exp. Optom*, vol. 91, pp. 207–225, 2008.

[13] S. Venkathesh, S. Guthrie, F. R Cruickshank, R. T. Bailey, W. S. Foulds, and W. R. Lee, "Thermal lens measurements in the cornea," *Brit. J. Ophthalmol.*, vol. 69, pp. 92–95, 1985.

[14] M. Hosney, J. L. Alio, P. Claramonte, W. H. Attia, and J. J. Perez-Santonja, "Relationship between anterior chamber depth, refractive state, corneal diameter, and axial length," *J. Refractive Surg.*, vol. 16, pp. 336–340, 2000.

Authors' photographs and biographies not available at the time of publication.